Formation of a periodic structure on the surface of InP crystal during irradiation with bismuth ions

Yu. Kudriavtsev[1], A. G. Hernandez[1], José Juan Diaz[1,*] ⓘ, M. Avendano[1], G. Ramirez[1], and R. Asomoza[1]

[1] *Solid State Electronics Section, Electrical Engineering Department, CINVESTAV-IPN, Av. IPN N. 2508, Col. San Pedro Zacatenco, 07360 Mexico City, Mexico*

ABSTRACT

This work is devoted to the study of the formation of periodic relief on the InP surface during ion sputtering by bismuth ions with an energy of 30 keV and an angle of incidence of 45° respect to normal incidence. We compared the reliefs formed by sputtering with atomic and cluster bismuth ions, as well as the relief appearing on the surface of the sample irradiated at elevated temperature (290 °C). Three different types of reliefs were found: surface waves with nanodots on the surface "waves", nanodots with uniform distribution and relief in the form of columnar micro crystallites during sputtering of a heated target. With increasing irradiation dose, insignificant changes in characteristic surface dimensions were observed for all three reliefs. Based on the nonlinear character of surface sputtering ("thermal spot" sputtering mode), we described the formation of relief in the form of nano-dots and in the form of micro crystallites as a result of local melting areas formation and subsequent solidification (crystallization) on the target surface. Regarding wave relief, in our opinion, an adequate physical description is given by a model based on the stress driven dynamics of ion irradiated surface.

1 Introduction

The formation of nano structured surfaces under irradiation of semiconductor crystals with accelerated ion beams has been actively studied in the last two decades due to some interesting optical (quantum dots and optically active nanostructure), photovoltaic (antireflection cover) and bioactive properties of such surfaces [1]. The literature contains extensive data on the formation of nano-dot relief, wave relief, nano- and micro pyramids, checkerboard relief, surfaces with etch pits, and foam-like surfaces [1–4]. Attempts to describe the physical mechanism of formation of various reliefs cannot yet be recognized as successful, at least from the point of view of predicting the type of relief formed on the target surface during ion irradiation by a given ion with a certain angle of incidence and ion energy. Wave topography is often described within the framework of the Bradley-Harper model, which uses the dependence of the sputtering velocity on the angle of incidence of ions relative to the normal [5]. Wave formation within the framework of this model is considered as a "competition" of increasing surface inhomogeneity as a result of different local sputtering

---

coefficients and surface diffusion compensating for the resulting element concentration gradient on the surface.

In our previous work we considered the mechanism of formation of nano dots, etch pits and foam-like surface [4]. We explained the formation of such reliefs by nonlinear effects of ion–solid interaction: the "temperature" of the cascade (defined as the average kinetic energy of recoil atoms in the cascade) for certain combinations of ion target and irradiation modes is so high that a local melt is formed, which in the process of solidification leads to the formation of nano-crystals or pores (depending on the material and irradiation mode) on the top or under the surface. Continuous irradiation leads to the formation of the above-mentioned reliefs.

In this work, a comparative analysis of the surface etching of InP crystals by atomic and cluster bismuth ions with 30 keV energy is carried out. Several studies of relief formation on the InP surface under ion irradiation have been published in the literature, however all of them were focused on low-energy sputtering mainly by inert gas ions with energies up to 5 keV [6–12]. The topography resulting from sputtering with medium-energy (20–100 keV) metal ions (typical mode for FIB systems and modern TOF–SIMS spectrometers) remains unexplored. The main objective of our experiments was to compare the obtained reliefs depending on the cascade density (or "cascade temperature") in the near-surface region of the target, including the dependence on the target temperature during irradiation.

1.1 Experimental

Experimental samples of 5 × 2 mm size were cleaved from standard undoped commercial InP substrates with orientation (100). Ion irradiation was carried out by Bi_1^+ and Bi_3^+ ions with energy of 30 keV. The angle of incidence was 45° relative to the normal to the surface. The sizes of irradiated areas ranged from 100 × 100 to 200 × 200 microns. The current density of Bi_1^+ ions ranged from 1.2×10^{13} ions·cm^{-2}s^{-1} to 1.5×10^{13} ions·cm^{-2}s^{-1}, and the ion current density of Bi_3^+ ions ranged from 0.8×10^{13} ions·cm^{-2}s^{-1} to 1.1×10^{13} ions·cm^{-2}s^{-1}. Such currents allowed us to study the initial stage of sputtering and relief formation developed at irradiation doses from 4×10^{15} ions/cm^2 to 8×10^{16} ions/cm^2. An additional experiment was performed with a current density of Bi_1^+ ions equal to 4.4×10^{13} ions·cm^{-2}s^{-1}. The second part of the InP ion etching experiments with bismuth ions was conducted when the target temperature was approximately 290 °C. This temperature was chosen to prevent the evaporation of phosphorus atoms from the InP surface to form an indium-enriched layer.

The structure of the etching surface was analyzed by the Atomic Force Microscope Solver Next of NT-MDT company. Both contact and semi-contact modes were used. The radius of curvature of the cantilevers used was approximately 10 nm. Processing of the obtained images was performed by the IA-P9 package from the microscope manufacturer.

Optical measurements of etch craters by Raman Spectroscopy were performed using a Ntegra Spectra spectrometer of NT-MDT company. A green laser (532 nm) was used; the beam was focused onto the surface using a × 100 objective.

Mathematical modeling of the penetration depth of primary ions and the energy released by them was carried out by the Monte Carlo method, using the SRIM-2008 program [13].

1.2 Experimental results

Figure 1 a-c shows the images of the etching surface obtained by AFM in the center of the etch crater with a beam of Bi_1^+ ions with energy 30 keV and different irradiation doses, the AFM micrographs are 5 × 5 microns. A wave structure conjugated with nano dots is observed, with the density of nano dots and their size increasing slightly with irradiation dose. The amplitude of the waves also increases. The wave period was approximately 185 nm for the structure shown in Fig. 1c, which is a typical value for wave reliefs produced by ion sputtering [1, 2].

Figure 1 d-f shows images of the 5 × 5 micron etching surface measured in the center of the etch crater by using a beam of Bi_3^+ bismuth cluster ions with the same energy as atomic bismuth ions. For all three irradiation doses, a relief in the form of nano dots was observed. We plotted the dependence of the size of nano dots on the time (dose) of irradiation: the data is shown in Fig. 2. The size of nano-dots grows rapidly accordingly to dose and reaches saturation.
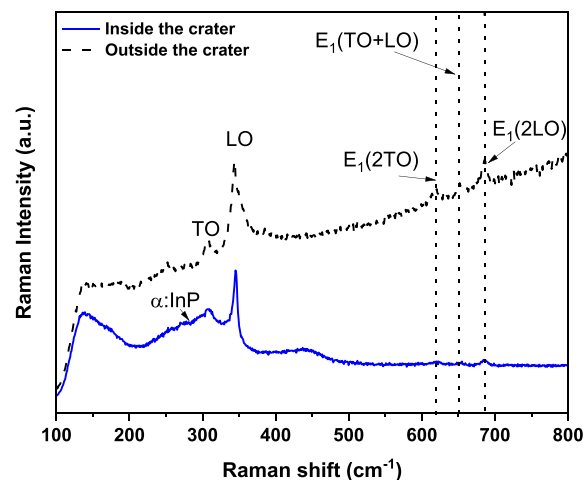
It is known that one of the results of ion irradiation of crystals is complete or partial amorphization of the near-surface layer. We used Raman spectroscopy to evaluate the degree of amorphization of the irradiated InP surface. Figure 3 shows spectra

Fig. 1 AFM images of InP surface sputtered with Bi_1^+ ions (**a**–**c**) and Bi_3^+ ions (**d**–**f**) for different sputter times (doses): 15 min or 1.1$\times 10^{16}$ ion/cm^2 for Bi_1^+ (**a**) and 7.3$\times 10^{15}$ for Bi_3^+ (**d**), 30 min or 2.2$\times 10^{16}$ ion/cm^2 for Bi_1^+ (**b**) and 1.45$\times 10^{16}$ for Bi_3^+(**e**), 60 min or 4.3$\times 10^{16}$ ion/cm^2 for Bi_1^+ (**c**) and 2.9$\times 10^{16}$ for Bi_3^+(**f**). The scan size is 5$\times$5 microns and the height (z) is indicated in each figure
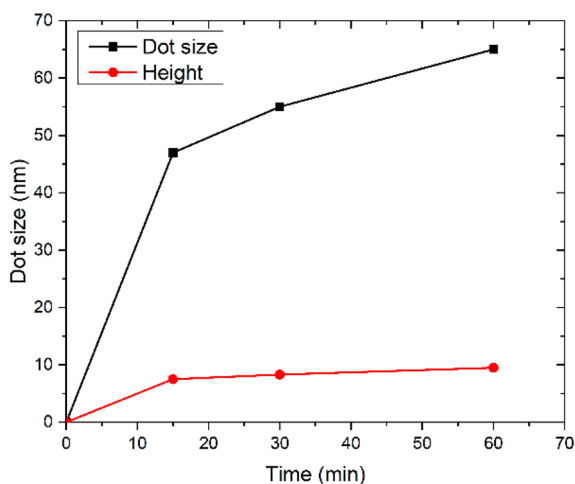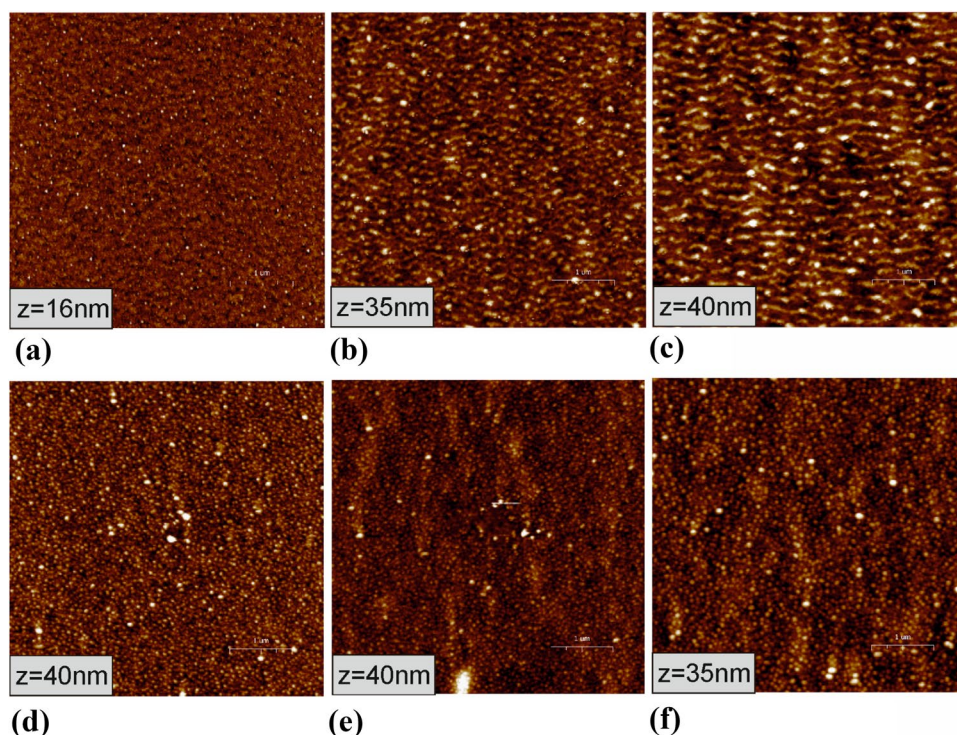
Fig. 2 Dependence of the size of nano dots formed during ion sputtering of InP on the sputter time (irradiation dose) for the images shown in Fig. 1a–c. The lines are a guide to the eye

Fig. 3 Raman spectrum of the bottom of the etching crater relief is shown in Fig. 1c in comparison with the spectrum obtained for the original InP surface

obtained on the original InP surface and inside the sputter crater, microscopic images of the surface of which are shown in Fig. 1c. While for the spectrum obtained outside the etching crater, the LO and TO vibrational modes are observed with the LO mode dominating and with the standard ratio for the modes (for a given InP crystal orientation),

in the case of the spectrum for the bottom of the etching crater, the signal of amorphous InP (in the 270–280 cm^{-1} region) is clearly registered. A new signal, usually associated with indium oxide, is also can be noted in the 140–150 cm^{-1} region. The latter suggests that part of the nanodots on the surface has a layer of metallic indium with a thin oxide film

formed in air during the transfer of the sample from one device to another [14–16].

In a number of works on ion irradiation of InP and formation of ordered relief on its surface, the effect of ion current density is noted: at the current density of argon ions with energy of 1.9 keV below about 1×10^{14} ions·cm^{-2}s^{-1}, nano dots are not observed, and above that, ordered nano dots appear on the whole surface [14]. In the above images for ion current densities "below critical" value, we nevertheless observe nanodots also at atomic ion sputtering (Fig. 1b–c); irradiation with cluster ions already at low doses show characteristic relief in the form of nano-dots despite the low ion current density. The observed difference, we believe, is due to a difference in the sputtering mode, namely the use of a very heavy bismuth ion, which forms denser collision cascades, with a higher temperature in the cascade than Ar$^+$ ions in the cited work [14]. The processes in collision cascades will be discussed in detail below.

We repeated the experiment with sputtering of the InP surface by Bi$_1^+$ ions with increased ion current density. We used an ion current density of 4.4×10^{13} ions·cm^{-2}s^{-1}, which is lower than the "critical current density" observed in the work cited above. Nevertheless, a characteristic topography in the form of nano dots in the absence of wave topography is observed, shown in Fig. 4a. At the same time, the size of the nano dots was found to be close to the size obtained by sputtering with Bi$_3^+$ ions with ion current density equal to about 1×10^{13} ions·cm^{-2}s^{-1}. The dependence of the dot size on the etching time (ion dose) is shown in Fig. 4b. For a dose equal to about 7.8×10^{16} ions/cm^2 a slight decrease in the size of nano

dots is observed compared to nano dots obtained with half the dose. This effect was observed previously in [12]. Since no other features were found in the obtained reliefs for sputtering with Bi$_1^+$ ions, we do not present the rest of the data here.

In previous works, devoted to the ion irradiation of InP and the formation of a regular relief on it, the effect of the target temperature on the relief obtained in the process of ion irradiation was noted [11, 14]. In this work, we studied the surface relief appearing on the InP surface during sputtering of a target heated to 290 °C. As in the previous experiment, the reliefs obtained by irradiation with Bi$_1^+$ and Bi$_3^+$ ions were compared.

Figure 5 shows three-dimensional (3-D) images of the 10×10 micron Bi$_1^+$ (a–c) and Bi$_3^+$ (d–f) ion etching surfaces obtained at different irradiation doses. This topography is radically different from that previously obtained. It consists of vertical crystallites with the top truncated at a certain angle (close to 45°), especially pronounced truncation of the top at sputtering with Bi$_1^+$ ions, whereas for Bi$_3^+$ the tops of crystallites look smooth. The crystallites are irregularly shaped, for large doses the base is wider than the middle and top, which is caused by ion etching with the effect of shading from nearby crystallites. The formed crystallites at the maximum used doses of ion etching have heights up to 1 micron and the sizes in the target plane reach ~500 and ~750 nm for the surface of irradiated Bi$_1^+$ and Bi$_3^+$, respectively. Statistical analysis of crystallite sizes is difficult due to the scatter in their height and irregular shape.

For clarity we also present images of the surfaces of the same etching craters obtained in the Lateral Forces

Fig. 4 AFM image of the crater bottom of InP etching with Bi$_1^+$ ions at a dose of 5.2×10^{15} ions/cm^2 (**a**). Dependence of the size of nanodots formed during etching of InP by Bi$_3^+$ ions on etching time (**b**). The ion current density was 4.4×10^{13} ions·cm^{-2} s^{-1}. The lines (**b**) are a guide to the eye
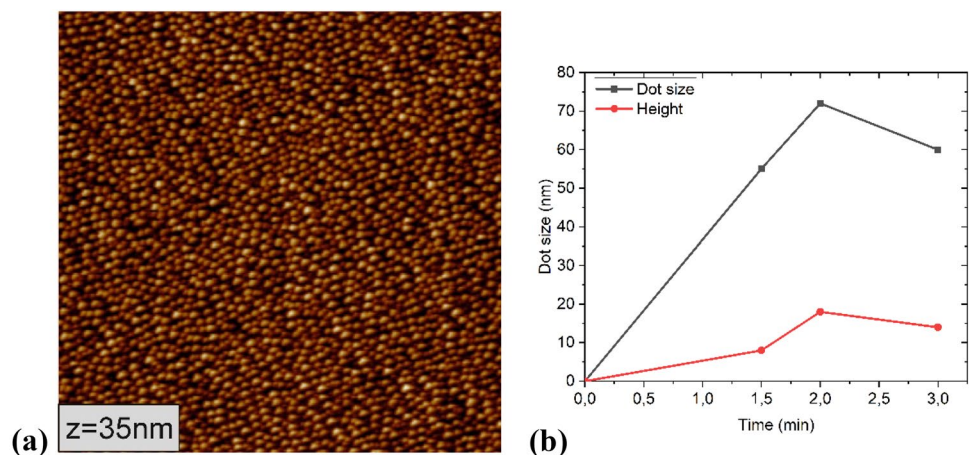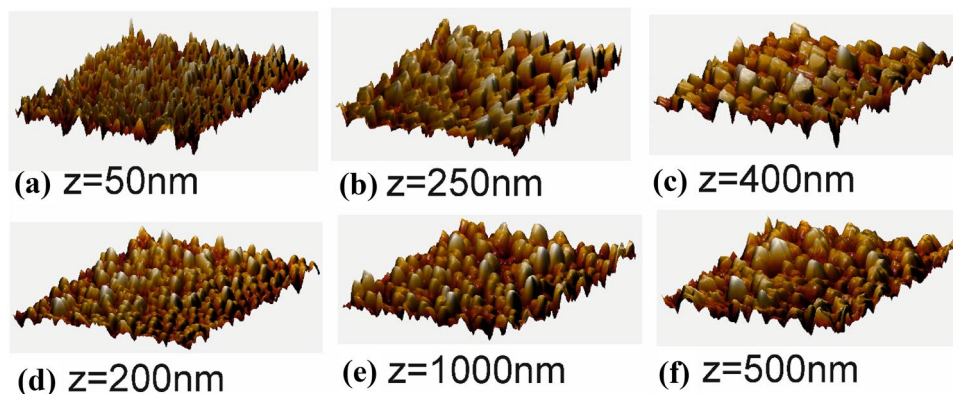
Fig. 5 3-D AFM images of the InP etch surface by Bi_1^+ ions (**a–c**) and Bi_3^+ ions (**d–f**) for different etch doses at a target temperature of 290 °C: 1.2×10^{16} ion/cm^2 (**a**), 2.7×10^{16} ion/cm2 (**b**), and 5.4×10^{16} ion/cm^2 (**c**) for Bi_1^+; and 9.5×10^{15} ion/cm^2 (**d**), 2.2 ion/cm^2 (**e**), and 3.8 ion/cm^2 (**f**) for Bi_3^+. The scan size is 10×10 microns, and the height (z) is given for each figure

Mode, see Fig. 6. In this mode, the surface relief looks like "fish scales", which is of course a distortion of the real relief. However, in this mode the triangular shape of crystallites (for Bi_1^+ sputtering) and their sizes are clearly visible, as well as the "fine structure" arising at higher doses: some secondary formations are visible on the surface of large crystallites, see Fig. 6l. Another

characteristic feature of the experiment is a very fast process of crystallite nucleation: they are clearly visible already at a dose of 4.5×10^{15} ion/cm^2, see Fig. 6i.

The bottom of sputter craters with Bi_3^+ ions at high temperature were studied with Raman spectroscopy. Figure 7 shows the spectra obtained for the three etching craters shown in Fig. 5 d, e and f. The Raman

Fig. 6 AFM images of Bi_1^+ (**a–d**) and Bi_3^+ (**e–h** and **i-l**) etch surfaces for different etching doses obtained in the "lateral forces" mode. The following doses were used: 6.2×10^{15} ion/cm^2 (**a**), 1.2×10^{16} ion/cm^2 (**b**), 2.7×10^{16} ion/cm^2 (**c**), and 5.4×10^{16} ion/cm^2 (**d**) for Bi_1^+; and 4.5×10^{15} ion/cm^2 (**e,i**), 9.5×10^{15} ion/cm^2 (**f,j**), 2.2×10^{16} ion/cm^2 (**g,k**), and 3.8×10^{16} ion/cm^2 (**h,l**) for Bi_3^+. The images correspond to the same experimental craters as those presented in Fig. 5, but the sizes of the scans presented in this figure are 5×5 microns for images (**a–h**) and 2×2 microns for images (**i–l**). The z scale in nA is indicated in each figure
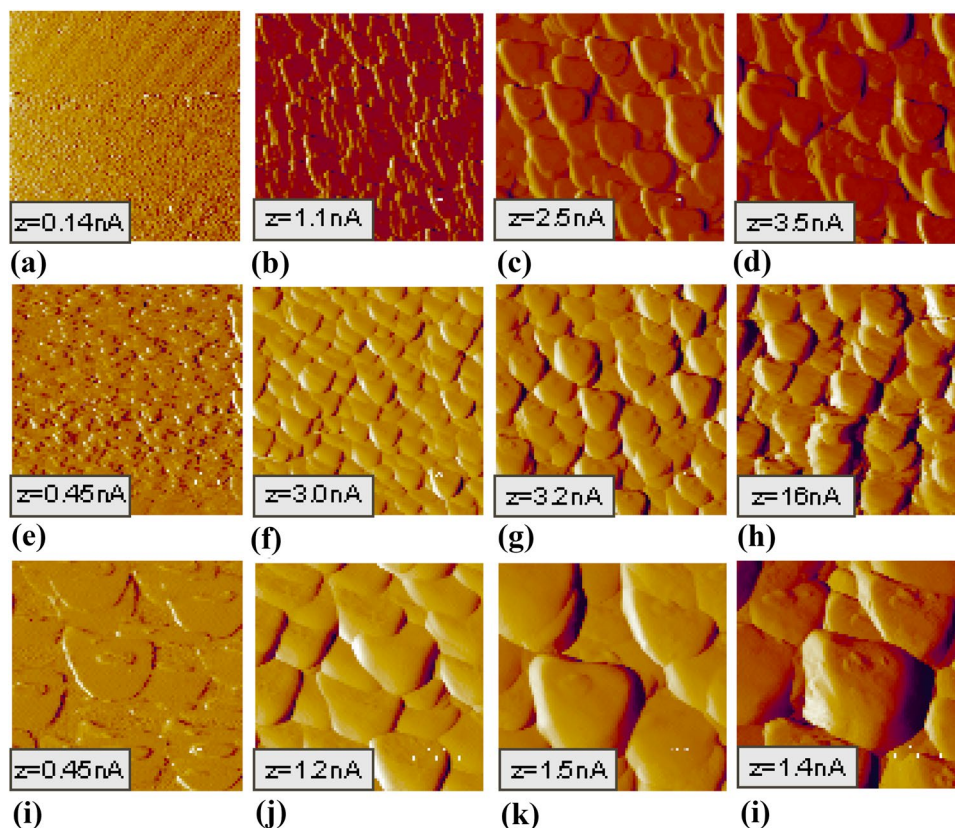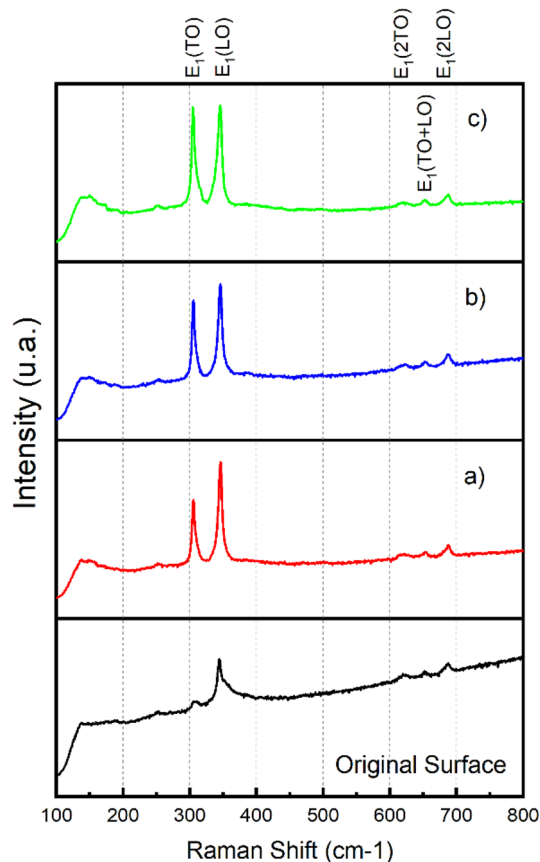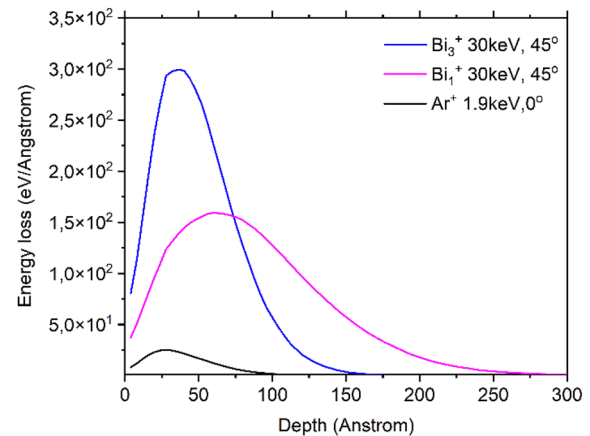
Fig. 7 Raman spectra of the bottom of the etch craters whose topography is shown in Fig. 5d (**a**), Fig. 5e (**b**) and Fig. 5f (**c**), compared to the original InP surface

Fig. 8 Energy losses of Bi_1^+ (30 keV), Bi_3^+ (30 keV) and Ar^+ (1.9 keV) ions in InP target as a function of depth, calculated by Monte-Carlo method; SRIM-2008 code

vertical crystallites with sizes up to 1 micron and base up to 750 nm at sputtering by both Bi_1^+ and Bi_3^+ ions.

1.3 Experimental result discussion

We begin the discussion with the wave relief on the surface of the irradiated target, shown in Fig. 1b,c. The appearance of wave relief in the ion sputtering regime we used is a rather unexpected result. As mentioned in the introduction, wave topography is usually considered within the Harper and Bradley (H–B) model [5], as a result of the dependence of the ion etch rate on the ion incidence angle. It is important to note that B-H model consider surface topography formation within the framework of the "linear cascades" sputtering model proposed by Sigmund [20]. In contrast, we consider sputtering by both single-atom and cluster bismuth ions as a nonlinear mode of sputtering (thermal spot mode [4]). The difference in the modes is easily shown by comparing the ion energy losses estimated using the Monte Carlo method, SRIM-2008 program [13] for both regimes. Figure 8 shows the distribution profiles of energy released by primary ions in the near-surface region of the target calculated for atomic ions and triatomic bismuth ions with energy of 30 keV, and argon ions with energy of 1.9 keV (sputtering mode used in [14]). In the case of Bi_3^+ clusters, we simply added up the contribution from the three cascades from atomic bismuth ions with an energy of 10 keV. The effect of using clusters in many cases is strongly nonlinear, i.e., the difference in the energy released

spectrum obtained outside the etching crater is also shown there for comparison. As can be seen from the above data, as the irradiation dose increases, the relative signal corresponding to the vibrational mode of the TO increases. As a result, for the maximum irradiation dose used, the TO and LO signals are similar.

Such Raman spectra as in Fig. 7a–c are usually observed for nanowire-type structures of InP [17, 18]. Another principal result of the analysis is the absence of peaks corresponding to the amorphous phase of InP for all considered irradiation doses. That is, the process of ion-induced crystallization in this sputtering regime dominates over the amorphization process. Such an effect was previously observed by us when bismuth ions irradiated the surface of a germanium crystal at a crystal temperature above 450 °C [19]: the surface turned out to be completely crystalline, also according to Raman spectroscopy data. That is, based on the obtained data, we can speak about the growth of

during sputtering by Bi_3^+ ions in the near-surface region may really be even larger. But even from the above data for sputtering with Bi_3^+ ions the energy released in a thin surface layer less than 10 nm thick is more than an order of magnitude higher than for sputtering with argon ions with an energy of 1.9 keV. For atomic bismuth ions, the energy density lost is half as much, but it is also 7 times greater than for argon ions.

We believe that in the case we consider (sputtering by atomic bismuth ions) the wave relief is obtained in a strongly nonlinear regime of ion sputtering. That is, the physical model of the formation of the observed waves should be different from the H-B model, namely, it is necessary to consider the collective motion of surface atoms during the development of the cascade and its relaxation. To explain this behavior, the model considered in [21] seems to be the most suitable. The authors of that work argue that residual stress induced by the ions is responsible for pattern formation and accounts for its long-time dynamics. Using a continuum framework, authors derive closed nonlinear evolution equations for the depth of the irradiated layer with novel terms associated with the spatial distribution of damage that builds up through sustained bombardment. Using numerical modeling, the authors were able to reproduce the main dynamical features of the surface wavers under the experimental conditions considered.

As for the appearance of nanodots on the wave surface, and the growth of their number with increasing irradiation dose, we should consider two possible types of nanodots: nanodots consisting of InP and arising as a result of the formation of surface relief, and nanodots consisting of metallic In, arising from the preferential sputtering of phosphorus atoms and the association of indium atoms into nanodots. Recall that in this way, authors of [22] explains the process of micro pyramid formation due to the emerging effect of selective sputtering of the InP surface with high doses, which has a higher sputtering coefficient than metallic indium. Also, the formation of metallic nanodots consisting of bismuth atoms previously implanted during surface irradiation cannot be excluded at all. Tthe Raman spectrum with a broad peak in the region 140–150 cm^{-1}, corresponding to indium oxide, speaks in favor of the appearance of metallic indium nanodots. However, as shown in [14], there may be simply a phosphorus depleted InP layer on the surface of InP nanodots, in which surface indium can oxidize in air. For a final clarification of the situation, additional studies using methods that are currently unavailable to us are required.

As for the description of InP nanodot formation within the framework of the thermal spot model proposed by our research group earlier [4], it is possible to explain the observed topography in Fig. 1d–f and its change with increasing irradiation dose quite simply at the qualitative level. If we assume that almost every cascade excited by the Bi_3^+ ion is nonlinear with a temperature exceeding the melting point of InP, then the sizes of the observed nano-spots should correlate with the effective sizes of the cascades or, more precisely, of the formed melts. From the calculation data shown in Fig. 8, we can roughly estimate the cascade size in width at the half-height of the Gaussians approximating the depth energy loss distribution obtained from this simulation. For irradiation with Bi_3^+ ions, such an estimate yields approximately ~ 60 nm, which correlates well with the size of the formed nanodots shown in Fig. 2. The observed variation in the sizes of nanodots is a variation in temperature for different cascades and, as a consequence, in the melt volume, which is characteristic of statistical processes. The growth of nanodot sizes with increasing irradiation dose requires some additional explanation.

We believe that a logical explanation for the growth of the size of nano dots is the experimentally discovered so-called "finite sizer" effect in the sputtering of micro- and nano-structured targets [23]. In the cited work, the yield of clusters at irradiation of a bulk target with a flat surface and a surface covered with ridges of a certain width (14 nm and 50 nm), comparable to the characteristic size of the cascade caused by ions in this material under the used irradiation regimes, was compared. In the case of irradiation of the nano-structured surface, a significantly higher yield of secondary cluster ions was observed compared to the original surface, which is a characteristic feature of a nonlinear cascade with a higher temperature in the cascade. The authors explained the observed effect by an increase in the density of energy released in the surface nanostructure when an ion enters it, due to reduced energy transfer from the formed cascade to the surrounding material (reduction of energy transfer channels).

In our case (surface with nano-dots), the nanoparticles formed at the initial moment of irradiation on the target surface have sizes close or

almost identical to the sizes of the cascade and the "melt" formed from it. In the subsequent moments of ion sputtering, when another ion hits the already formed surface nano-particle, the temperature of the cascade in it increases much more than in the melt formed on the initially "flat" surface due to the reduction in the first hundreds of fs (of the cascade development time) of the channels of energy transfer from the cascade to the surrounding crystal. The re-formed melt due to the higher temperature partially "melts" the surrounding material, increasing the size of the melt and, consequently, the size of the "new" nanoparticle formed during solidification. The effect obviously tends to saturation, which we observe in Fig. 2 and has been mentioned in the literature [1, 12, 14, 15, 24].

The effect of nanodot size reduction at higher ion current fluence observed in Fig. 4b requires further investigation. The authors of reference [12] observed a similar effect when etching with Ar^+ ions with an energy of 3 keV, they explained the effect of increasing the size of nanodots by the growth of stress in the near-surface layer and relaxation of this stress during surface amorphization at a critical irradiation dose. From several early works on GaSb and Ge sputtering, it is known that nanodots have a crystalline structure with a thin amorphous layer on the surface [25, 26]. In [26] it was shown that with increasing temperature of the germanium target the Young's modulus of the surface irradiated by bismuth ions with an energy of 20 keV grows from 5 GPa at RT to 40 GPa at 350 °C, i.e. from the value typical for amorphous porous germanium to the value of the Young's modulus close to crystalline germanium. Note in this case for the value we need to take into account the decrease of the Young's modulus of Ge (both crystalline and amorphous) with increasing temperature compared to room temperature. In our case, as shown above, at low temperatures and low ionic current density, an amorphized layer remains on the surface, surrounded by InP nanodots. With increasing temperature and/or ion current density, the amorphous part decreases and at the "critical temperature" or at the "critical dose", complete crystallization of the surface occurs. That results, among other, to better energy transfer from melts to surrounding crystal. The phase transition-induced surface reconstruction leads, in our opinion, to a partial reduction in the size of the nanodots, as well.

The situation with relief in the form of large crystallites at irradiation of a target heated to 290 °C is a logical continuation of the development of relief consisting of nanodots according to the just discussed mechanism of solidification of local melts. The increased temperature of the target leads to significant increase of the lifetime of the melt. Molecular dynamics simulations for the sputtering of metals by argon ions with energies of 2–5 keV give estimates of the lifetime of local melts in metals on the order of 20–50 ps, depending on the ion and the type of target [27–29]. But what will happen to the melt if its temperature is much higher than that obtained in the cited works? This question can be answered by an experiment on laser irradiation of a silicon target [30].

The authors of reference [30] used an original design to measure the time of melt emergence and solidification when a femto-second pulse is irradiated on a silicon surface using a second femto-laser. The reflection coefficient of the solid silicon surface and the silicon melt are significantly different, which allowed the authors to reliably record both the moment of melt formation and solidification. If the formation of the melt (if melting occurs) for all used powers in the laser pulse is approximately the same and is equal to about 0.5 ps, then for the time of solidification, the dependence on the pulse power, and thus on the released energy in the near-surface layer, varies greatly. For a laser pulse with an energy of 0.25 J/cm^2, the time of melt existence is already about 1 ns, and at an energy of 0.29 J/cm^2 solidification does not occur after 3 ns! As can be seen from the modeling results, when the InP surface is irradiated with Bi_3^+ ions, the energy released at the surface is much higher than when irradiated with argon ions. And if at irradiation with argon ions with energy of 1.9 keV we also observe relief in the form of nanodots [14], i.e. formation of melts, then for irradiation with bismuth ions at elevated target temperature, we have every reason to assume a significant increase in both the melt temperature and the time of their solidification. The increased temperature of the melt leads to its increase in size (compared to nano-dots at room temperature). And the increase by several orders of magnitude of the melt lifetime leads to the possibility of overlap of two or more melts formed by different primary ions. Thus, the melts and the crystallites arising after solidification significantly increase in size, which we observe in Figs. 5 and 6. Continuing the same logic, we can assume that a further increase

in the target temperature can lead to the fact that the entire irradiated surface area (etching crater) will turn into a melt, which will solidify (crystallize) after the ion beam is turned off. This is exactly the result we observed in the experiment on ion irradiation of germanium crystal with bismuth ions [19]: when the target temperature was increased to 450 °C, a checkerboard-like relief was formed on the target surface, and the Raman spectrum obtained for the etching surface coincided with the spectrum of the original germanium single crystal. That is, there was a complete crystallization of the surface of the bottom of the etching crater under ion irradiation.

2 Conclusions

This paper presents the results of analyzing the surface topography obtained by irradiation of InP crystals surface with atomic and cluster Bi ions with 30 keV energy at different target temperature.

To explain the wave topography during sputtering of InP at room temperature by atomic ions, we used the model of Muñoz-García and co-authors, which considers the collective motion of surface atoms caused by the surface tension induced by primary ions.

Upon irradiation of the surface with Bi_3^+ ions, a characteristic relief in the form of nanodots is observed, the size of which grows with increasing dose and quickly reaches saturation at a dose of the order of 2×10^{16} ions/cm^2. We explain this relief in the form of InP nanodots by the formation of local melts from nonlinear cascades and their subsequent solidification.

We explained the growth of the nanodot size with increasing ion fluence by the effect of "finite size" arising in the previously formed surface nanodots, when bombarded by the primary ion, due to the reduction of the channels of energy transfer from the cascade to the surrounding crystal.

The formation of relief in the form of crystallites up to 1 μm in size on the InP surface when the target is heated to 290 °C is also explained by the formation of local melts. Increasing the temperature of the target leads to the fact that the melt temperature and, accordingly, the lifetime of such a melt strongly increase. Both the first and the second leads to an increase in the size of the melts. And the lifetime of a melt at a sufficiently high temperature of the latter can exceed the lifetime of a "low-temperature" melt by more than three orders of magnitude, as follows from experiments with laser melting of the silicon surface. This, in turn, may lead to the overlap of nearby melts formed from cascades formed by different primary ions.

Based on this logic, we conclude that with a further increase in the target temperature, we can observe melting followed by crystallization of the surface of the entire InP etch crater.

Acknowledgements

Funding

Declarations

Competing interests The authors have not disclosed any competing interests.

References

1. B. Rauschenbach, *Low-energy ion irradiation of materials. Fundamentals and application. Springer series in materials science* (Springer, Cham, 2022)

2. H. Bernas, *Materials science with ion beams, in topics in applied physics* (Springer-Verlag, Berlin, 2010)

3. J. Muñoz-Garcia, L. Vazquez, R. Cuerno, J.A. Sanchez-Garcia, M. Castro, R. Gago, Self-organized surface nano patterning by ion beam sputtering, in *Toward functional materials*. ed. by Z.M. Wang (Springer, New York, 2009)

4. Y. Kudriavtsev, R. Asomoza, A. Hernandez, D.Y. Kazant-sev, B.Y. Ber, A.N. Gorokhov, J. Vac. Sci. Technol. A **38**, 053203 (2020). https://doi.org/10.1116/6.0000262

5. R.M. Bradley, J.M.E. Harper, Theory of ripple topography induced by ion bombardment. J. Vac. Sci. Technol. A **6**, 2390 (1988). https://doi.org/10.1116/1.575561

6. S.K. Tan, A.T.S. Wee, Self-organized nanodot formation on InP (100) by argon ion sputtering at normal incidence. J. Vac. Sci. Technol. B **24**, 1444 (2006). https://doi.org/10.1116/1.2203643

7. J.B. Malherbe, Sputtering of compound semiconductor surfaces: II. Compositional changes and radiation-induced topography and damage. Crit. Rev. Solid State Mater. Sci. **19**, 129 (1994). https://doi.org/10.1080/10408439408244589

8. C.M. Demanet, J.B. Malherbe, N.G. van der Berg, V. Sankar, Atomic force microscopy investigation of Argon-bombarded InP: effect of ion dose density. Surf. Interf. Anal. **23**, 433 (1995). https://doi.org/10.1002/sia.740230702

9. M.M. Sung, S.H. Lee, S.M. Lee, D. Marton, S.S. Perry, J.W. Rabalais, Composition and morphology of InP(100) surfaces as a function of low energy Ar+ bombardment and annealing. Surf. Sci. **382**, 147 (1997). https://doi.org/10.1016/S0039-6028(97)00118-0

10. C.M. Demanet, K.V. Sankar, J.B. Malherbe, N.G. van der Berg, R.Q. Odendaal, Atomic force microscopy investigation of noble gas ion bombardment on InP: effect of ion energy. Surf. Interf. Anal. **24**, 497 (1996). https://doi.org/10.1002/(SICI)1096-9918(199608)24:8%3c497::AID-SIA143%3e3.0.CO;2-K

11. J.B. Malherbe, Bombardment-induced ripple topography on GaAs and InP. Nucl. Instrum. Methods. Instrum. Methods **B212**, 258 (2003). https://doi.org/10.1016/S0168-583X(03)01454-X

12. D. Paramanik, S.N. Sahu, S. Varma, Morphological evolution of InP nano-dots and surface modifications after keV irradiation. J. Phys. D Appl. Phys. **41**, 125308 (2008). https://doi.org/10.1088/0022-3727/41/12/125308

13. www.srim.org

14. T. Radny, H. Gnaser, Self-organizing nanodot structures on InP surfaces evolving under low-energy ion irradiation: analysis of morphology and composition. Nanoscale Res. Lett. **9**, 403 (2014)

15. I. Sulania, P. Kumar, P.K. Priya, H.P. Bhasker, U.B. Singh, R.K. Karn, C. Tyagi, R.P. Yadav, Formation of self-organized nano-dimensional structures on InP surfaces using ion irradiation and their wettability: a study based on experimental and theoretical concepts of surface. Rad. Phys. Chem. **199**, 110353 (2022). https://doi.org/10.1016/j.radphyschem.2022.110353

16. I. Sulania, D.C. Agarwal, M. Kumar, S. Kumar, P. Kumar, Topography evolution of 500 keV Ar+4 ion beam irradiated InP (100) surfaces – formation of self-organized In rich nano-dots and scaling laws. Phys. Chem. Chem. Phys. **18**, 20363 (2016). https://doi.org/10.1039/C6CP03409H

17. J. Park, C.H. Chung, Raman spectroscopic characterizations of self-Catalyzed InP/InAs/InP one-dimensional nanostructures on InP(111)B substrate using a simple substrate-tilting method. Nanoscale Res. Lett. **14**, 355 (2019). https://doi.org/10.1186/s11671-019-3193-6

18. J.H. Park, M. Pozuelo, B.P.D. Setiawan, C.-H. Chung, Self-catalyzed growth and characterization of In(As)P nanowires on InP(111)B using metal-organic chemical vapor deposition. Nanoscale Res. Lett. **11**(1), 1–7 (2016). https://doi.org/10.1186/s11671-016-1427-4

19. A.G. Hernández, Yu. Kudriavtsev, Bim+ ion beam patterning of germanium surfaces at different temperatures and ion fluence. J. Vac. Sci. Technol. B **34**, 061805 (2016). https://doi.org/10.1116/1.4967697

20. P. Sigmund, Sputtering by ion bombardment theoretical concepts, in *Sputtering by particle bombardment I*. ed. by R. Behrisch (Springer-Verlag, Berlin, 1981), pp.9–72

21. J. Muñoz-García, R. Cuerno, M. Castro, Stress-driven nonlinear dynamics of ion-induced surface nanopatterns. Phys. Rev. B **100**, 205421 (2019). https://doi.org/10.1103/PhysRevB.100.205421

22. S.W. MacLaren, J.E. Baker, N.L. Finnegan, C.M. Loxton, Surface roughness development during sputtering of GaAs and InP: evidence for the role of surface diffusion in ripple formation and sputter cone development. J. Vac. Sci. Technol. A **10**, 468 (1992). https://doi.org/10.1116/1.578173

23. A.B. Tolstoguzov, M.N. Drozdov, A.E. Ieshkin, A.A. Tatarintsev, A.V. Myakon'kikh, S.F. Belykh, N.G. Korobeishchikov, V.O. Pelenovich, D.J. Fu, Influence of the finite-size effect on the cluster ion emission of silicon nanostructures. J. Exp. Theor. Phys. Letters **111**(8), 467–471 (2020). https://doi.org/10.1134/S0021364020080123

24. I. Sulania, D.K. Avasthi, A. Tripathi, M. Hussain, Nanopattern formation on indium phosphide using energetic ions: an overview with various ion beam parameters. ECS Trans. **107**(1), 3107–3116 (2022)

25. S. Facsko, T. Dekorsy, C. Trappe, H. Kurz, Self-organized quantum dot formation by ion sputtering. Microelectron. Eng.. Eng. **53**, 245–248 (2000). https://doi.org/10.1016/S0167-9317(00)00307-5

26. R. Bottger, A. Keller, L. Bischoff, S. Facsko, Mapping the local elastic properties of nanostructured germanium surfaces: from nanoporous sponges to self-organized nanodots. Nanotechnology **24**, 115702 (2013). https://doi.org/10.1088/0957-4484/24/11/115702

27. T. Diaz De La Rubia, R.S. Averback, R. Benedek, W.E. King, Role of thermal spikes in energetic displacement cascades. Phys. Rev. Lett. **59**, 1930 (1987). https://doi.org/10.1103/PhysRevLett.59.1930

28. T. Diaz De La Rubia, M.W. Guinan, New mechanism of defect production in metals: a molecular-dynamics study of interstitial-dislocation-loop formation in high-energy displacement cascades. Phys. Rev. Lett. **66**, 2766 (1991). https://doi.org/10.1103/PhysRevLett.66.2766

29. K. Nordlund, S.J. Zinkle, A.E. Sand, F. Granberg, R.S. Averback, R.E. Stoller, T. Suzudo, L. Malerba, F. Banhart, W.J. Weber, F. Willaime, S.L. Dudarev, D. Simeone, Primary radiation damage: a review of current understanding and models. J. Nucl. Materials **512**, 450–479 (2018). https://doi.org/10.1016/j.jnucmat.2018.10.027

30. A.A. Ionin, S.I. Kudryashov, L.V. Seleznev, D.V. Sinitsyn, V.N. Lednev, S.M. Pershin, J. Exp. Theor. Phys.Theor. Phys. **121**, 737 (2015). https://doi.org/10.1134/S1063776115110143X